

Photo-birefringent effects in crystalline AlGaAs mirror coatings

C. Y. Ma, J. Yu, T. Legero, S. Herbers, D. Nicolodi, M. Kempkes, F. Riehle and U. Sterr
Physikalisch-Technische Bundesanstalt, Bundesallee 100, 38116 Braunschweig, Germany
(Dated: February 5, 2026)

High-reflective crystalline GaAs/Al_{0.92}Ga_{0.08}As coatings show reduced Brownian noise compared to conventional dielectric coatings. However, several ultra stable laser systems observed additional noise sources that hinder the realization of the expected improvements in frequency stability. These additional noise sources are related to the birefringence of the coatings and its modification by intracavity light. The origin of the birefringence is not yet well understood and its modification via illumination remains unexplained. Here we present an extensive study on the steady-state and transient modification of the birefringence by intracavity light and by uniform illumination at various wavelengths using an optical cavity at room temperature. We find a unified description that suggests a primary two-photon process for photon energies below the bandgap of GaAs, or a single-photon process at higher energies. Adding external illumination allows to reduce noise induced by laser power fluctuations by balancing the photo-thermal-optic response of the mirrors and the photo-birefringent effect at a more favorable low intracavity power.

I. INTRODUCTION

Ultra-high reflectivity mirror coatings are indispensable for Fabry-Perot cavities required for optical atomic clocks [1] or for gravitational wave detectors [2]. In these state-of-the-art instruments, the frequency or length stability is fundamentally limited by Brownian thermal noise of the mirror coatings [2, 3]. The Brownian thermal noise can be reduced using materials with smaller mechanical loss: crystalline AlGaAs coatings exhibit Brownian thermal noise power spectral density 16 times smaller than conventional dielectric coatings. This has been confirmed in both room-temperature and cryogenic cavities [4, 5]. However, ultra stable cavities with these coatings showed additional noise contributions [5, 6] related to the so far not well understood birefringence of the coatings. In ultra stable cavities operating at 1070 nm, 1397 nm and 1542 nm, it has been observed that the birefringence of the coatings can be modified by intracavity light [5–9]. It was also observed that the coating birefringence can be modified with illumination [9, 10]. In reference [9] a 500 Hz shift was observed at an intracavity power level of 1 W or at about 100 nW for diffuse light at 450 nm reaching the area of the coating.

Understanding the underlying mechanism of these effects might help to optimize next generation of crystalline coatings. In this work we employ a room-temperature ultra low expansion glass (ULE) cavity with fused silica substrates and crystalline coatings. We investigate the responses of the coating birefringence to intracavity radiation at 1542 nm and to diffuse radiation at wavelengths between 450 nm and 890 nm. We can describe the modification of the birefringence with a single effect driven by a one or two photon absorption process depending on the wavelength. To study the dynamics of this effect we investigated the temporal response of the birefringence to step change of intracavity power. We offer an empirical model that takes into account the effect of intracavity power and additional uniform illumination.

The sensitivity of the coating birefringence to intra-

cavity power couples the cavity resonance frequencies to laser power fluctuations and hence induces frequency noise. Power fluctuations also change the frequency by thermal effects in the substrate and coating (photo-thermo-optic effect), which is significant for fused silica substrates commonly employed in room temperature cavities. It has been demonstrated that by choosing a suitable polarization, both effects could be largely canceled at a certain intracavity power [7, 8]. Our model well predicts the response with additional LED light. This allows to cancel both effects at low intracavity power where the absolute intracavity power fluctuations are smaller and thus the related frequency stability is improved.

II. EXPERIMENTAL SETUP

We study AlGaAs coatings with a room temperature resonator operating at 1542 nm, which is a copy of a previous cavity using dielectric coatings at 698 nm [11]. This design employs a 48 cm long ULE spacer and a pair of 25.4 mm diameter fused silica substrates (one plane and one concave with 1.0 m radius of curvature). AlGaAs coatings with 6 mm diameter [12] are bonded onto the substrates. They consist of 38.5 pairs of alternating Al_{0.92}Ga_{0.08}As/GaAs layers, of thickness 133.2 nm and 115.6 nm respectively, starting and ending with a GaAs layer. The $1/e^2$ beam radii at the plane mirror and at the concave mirror are 496 μm and 675 μm respectively. ULE rings are attached to the back of the mirrors to compensate for the coefficient of thermal expansion (CTE) mismatch between ULE and fused silica [13], leading to a measured CTE zero crossing at 297 K [9]. Similar to other optical resonators with AlGaAs coatings [5, 6, 8, 14], we align the birefringent axes of the mirrors, hence maximizing the frequency splitting Δ_{biref} between the two polarization eigenmodes (fast and slow) of 104 kHz. This corresponds to a birefringence $\Delta n_{\text{biref}} = \frac{\Delta_{\text{biref}}}{2\nu} \frac{L_{\text{cav}}}{l_{\text{pen}}} \approx 4.5 \times 10^{-4}$, where Δ_{biref} is the frequency splitting between the two axes, $\nu = 194.43$ THz is the

operating frequency of the resonator, L_{cav} is the optical length of the cavity, $l_{\text{pen}} = 286$ nm is the penetration depth of the light field in the optical coatings and the factor 2 accounts for the pair of mirrors in the resonator [15].

Two lasers are locked independently from opposite sides of the cavity each to a fundamental Hermite–Gaussian (HG_{00}) mode [5, 9] that are separated by one free spectral range of 312 MHz. The cavity finesse of an HG_{00} mode is $1.290(2) \times 10^5$ and $1.282(2) \times 10^5$ for slow and fast axis, respectively. The frequency difference between adjacent cavity modes is largely immune to fluctuations of the cavity resonant frequency.

The beat signal between the two lasers is detected from the transmitted and reflected beam at one side of the cavity. This common-path geometry avoids influence from path length fluctuations. This facilitates the study of coating specific photo effects that modify their birefringence.

The average frequency of the two lasers can be calculated from an additional optical beat with another single crystalline silicon cavity operated at 124 K with a frequency stability at 4×10^{-17} [16]. The average of the two frequencies removes anti-correlated frequency changes due to mirror birefringence on the mirrors. This enables investigations of polarization-independent effects such as the photo-thermo-optic effect.

Fig. 1 shows the experimental scheme. Diffuse light from a LED enters the vacuum system through one of the optical windows used for coupling laser light to the cavity and hits the near-end mirror after transmitting through two more windows on the heat shields. LEDs with wavelengths of 450 nm, 535 nm, 625 nm or 890 nm were used. It illuminates the rear side of the AlGaAs coating through the fused-silica substrate. From the geometry and the optical transmission of all three windows we can estimate the intensity I_{LED} at the back of the near-end AlGaAs coating.

As the original setup was not designed for this purpose, LED light also leaks through the uncoated area of the mirror and reaches the front surface of the far-end AlGaAs coating with a smaller intensity.

III. STEADY-STATE MODIFICATION OF LINE SPLITTING

Previously we presented preliminary data of the sensitivity of birefringence to 1542 nm intracavity light or to diffuse LED light [9]. We found a much higher sensitivity for light above the bandgap of GaAs. In addition, we have observed that the birefringent splitting Δ_{biref} from LED illumination at constant intracavity power can be described by a generic curve that only depends on the scaled intensity [9]. Here we develop a comprehensive description of the birefringence modification by the simultaneous actions of 1542 nm intracavity light and diffuse LED light. To this end we measure the birefringence re-

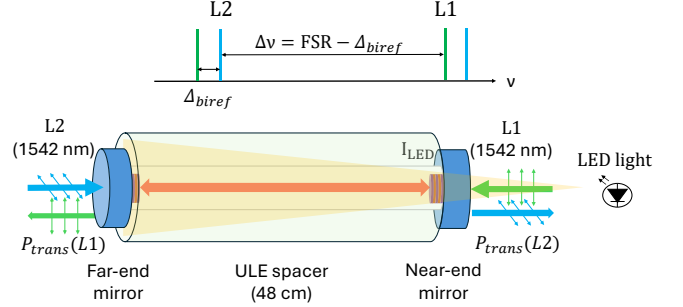


FIG. 1. Experimental scheme. Two lasers (L1 and L2) at 1542 nm are locked to eigenmodes of the ULE cavity separated by one free spectral range (FSR). Their polarizations are aligned with the slow and fast axes of the mirrors respectively. $P_{\text{trans}}(L1/L2)$ is the transmission power from individual lasers and I_{LED} is the LED intensity at the near-end mirror. The LED illuminates the back side of the AlGaAs coating on this mirror. Light that passes the uncoated area propagates 48 cm and illuminates the front surface of the far-end mirror coating with a smaller intensity.

sponse to different intracavity power, LED intensity and LED wavelength. The LED intensity is described by the intensity I_{LED} at the mirror that is close to the LED [9]. We use the sum of transmission power from the two independent lasers $L1$ and $L2$ $P_{\text{trans}} = P_{\text{trans}}(L1) + P_{\text{trans}}(L2)$ as proxy for the intracavity power $P_{\text{int}} = P_{\text{trans}}/T$ where $T = 15$ ppm is the design mirror transmission.

It was observed that the behavior of birefringent modification by intracavity and by short wavelength LED illumination as function of intensity is strongly different [9]. We advance the hypothesis that light with photon energies below the GaAs bandgap modifies the line splitting by an initial two photon absorption process where the effect scales with the square of the optical power, in contrast to single photon absorption for above bandgap light. To test this hypothesis, we plot the data as function of $(P_{\text{trans}}/P_0)^2$ and I_{LED}/I_0 in the same graph (Fig. 2). Without being able to derive the sensitivity coefficients from first principles, we can achieve a good agreement by applying the LED wavelength-dependent coefficient I_0 , such that $I_{\text{LED}} = I_0$ leads to a shift equal to the one induced by an intracavity power corresponding to $P_{\text{trans}} = P_0 = 1 \mu\text{W}$ (corresponding to intracavity intensity of $8.6 \times 10^4 \text{ W m}^{-2}$ on the plane mirror).

The observed correspondence between LED intensity and intracavity power squared indicates that the birefringence change can be modeled with two different initial processes driving a common mechanism. The following common process could modify the birefringence via the linear electro-optic effect in GaAs [17] from local electric fields. Another possible explanation could be the softening of GaAs on illumination (photo-plastic effect [18, 19]) due to relaxation of carriers at dislocations. As anisotropic stress relaxation was thought to be responsi-

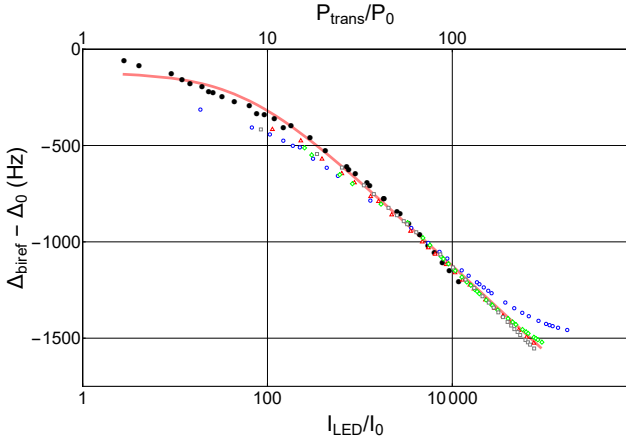


FIG. 2. Birefringent linesplitting Δ_{biref} as a function of normalized transmitted power P_{trans}/P_0 (black dots, top axis) with $P_0 = 1 \mu\text{W}$, and by diffuse LED light as a function of the scaled LED intensity (bottom axis) at $P_{\text{trans}} = 7 \mu\text{W}$. Values of the bottom axis are top axis values squared. The red curve shows a fit of Eq. 2 to the 1542 nm data. The scaling factors for LED amount to $I_0 = 14.3, 5.7, 3.4$ and $2.9 \mu\text{W m}^{-2}$ at the wavelength of 450 nm (blue circles), 625 nm (red triangles), 535 nm (green rhombs), and 890 nm (brown squares). For clarity, a fixed offset of $\Delta_0 = 104.280 \text{ kHz}$ was subtracted in the displayed y-axis.

ble for the static birefringence [20], the observed change of birefringence might also be explained by a modification of the stress built up in the coating.

We assume, that the observed change in birefringence can be expressed by one function $\Delta_{\text{biref}}(x)$ with a single argument

$$x = \frac{I_{\text{LED}}}{I_0(\lambda)} + \frac{P_{\text{trans}}^2}{P_0^2}. \quad (1)$$

As model for the line splitting function we try the Shockley diode equation [21] that relates the voltage to the current flowing through a p-n junction. In our case the current could be a photocurrent induced by the absorbed light that then modifies the birefringence by the corresponding charge distribution or electric fields:

$$\Delta_{\text{biref}}(x) = \Delta_{\text{biref}}^0 + \Delta_s \ln \left(\frac{x}{x_s} + 1 \right), \quad (2)$$

where Δ_{biref}^0 is the dark value of the line splitting. Δ_s and x_s are scaling factors for the induced shift and the light related quantity x .

A fit of this model to the shift Δ_{biref} induced by 1542 nm intracavity light is shown in Fig. 2. From the fit we obtain $\Delta_{\text{biref}}^0 = 104.26(1) \text{ kHz}$, $\Delta_s = -193(7) \text{ Hz}$, and $x_s = 56(10)$.

Because the LED is illuminating the two mirrors quite differently, we need to separate the contribution of the two mirrors to the modification of birefringence. We assume that the light-induced modification of the birefringence in the mirror material is mostly a local effect, which

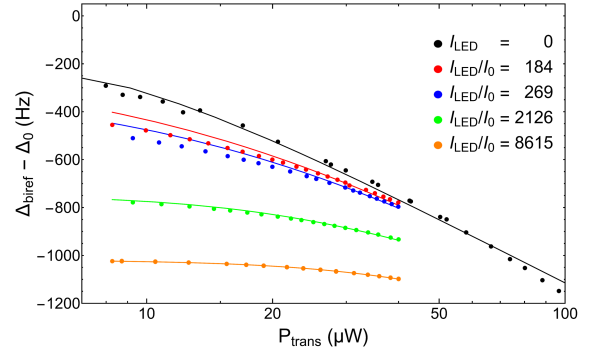


FIG. 3. Birefringent line splitting Δ_{biref} as a function of transmission power P_{trans} at different intensities of a green LED emitting at 535 nm. Eq. 3 was fitted to data at the highest LED intensity $I_{\text{LED}}/I_0 = 8615$ (orange line) to determine the ratio of effective LED intensities at both mirrors. The curves (green, blue and red) show the model using this ratio. For clarity, a fixed offset of $\Delta_0 = 104.280 \text{ kHz}$ was subtracted in the displayed y-axis.

implies a dependence on the local intensity at the mirror for both the intracavity 1542 nm light and the LED light. Assuming similar sensitivity of each mirror to the local intensities, the observed splitting is the sum of the two mirror contributions:

$$\Delta_{\text{biref}}(P_{\text{trans}}, I_{\text{LED}}) = \Delta_{\text{biref}}^0 + \Delta_s \left(\ln \left(\frac{x_{\text{near}}}{x_s} + 1 \right) + \ln \left(\frac{x_{\text{far}}}{x_s} + 1 \right) \right) \quad (3)$$

with

$$\begin{aligned} x_{\text{near}} &= P_{\text{trans}}^2/P_0^2 + I_{\text{LED}}/I_0(\lambda) \\ x_{\text{far}} &= \rho P_{\text{trans}}^2/P_0^2 + \eta I_{\text{LED}}/I_0(\lambda). \end{aligned} \quad (4)$$

For the intracavity light the $1/e^2$ mode radii w at the two mirrors differ significantly ($w_{\text{concave}} = 675 \mu\text{m}$, $w_{\text{plane}} = 496 \mu\text{m}$) leading to ratio of the intensities of 1.85 and thus to a factor $\rho = 1/3.6$ in the argument x . The influence of LED light on the far-end mirror is described by an effective intensity at the far end mirror $I_{\text{LED}}^{\text{far}}$. It is related to the intensity I_{LED} at the near end mirror by a factor η . This factor contains the divergence of the light and the different birefringence sensitivity when the far-end coating is illuminated from the front compared to back illumination of the coating on the near-end mirror.

We measure Δ_{biref} as a function of intracavity power at various LED intensities (Fig. 3). The rear side of the plane mirror was irradiated with a green LED ($\lambda = 535 \text{ nm}$), where $I_0(535 \text{ nm}) = 3.4 \mu\text{W/m}^2$ was determined previously.

First, we fit the model (Eqs 3, 4) to the observed shift at the highest LED intensity (Fig. 3, orange circles). We obtain a factor $\eta = 5.6(1)$, i.e. the effective intensity at the far mirror is 5.6 times bigger than the intensity I_{LED} at the mirror next to the LED. This is unexpected, as

from the 48-cm separation and the divergence, the light intensity at the far end mirror coating is at least an order of magnitude smaller. We suppose that the larger effective intensity is due to the larger sensitivity of the far end mirror coating that is illuminated from the front, in contrast to the rear-side illumination of the near-end mirror coating. In the far end mirror visible LED light is mainly absorbed in the first few layers within the penetration depth (see Table I in the Supplementary Material), where the birefringence is probed by the intracavity light. Thus the effect of the LED light can be much bigger.

With this ratio, we model the response to P_{trans} at other LED intensities using Eq. 3, as shown in Fig. 3. The fair agreement between the experimental data and the model supports the assumption that effects from both intracavity light and external LED light are simply additive to the intermediate quantity x that nonlinearly modifies the line splitting.

IV. TRANSIENT RESPONSE TO INTRACAVITY POWER

The temporal response of Δ_{biref} to a step change in intracavity power provides further insight into the mechanisms and also relates to frequency noise induced by fluctuations of intracavity power. Previously it was observed that the transient response of Δ_{biref} strongly varies with temperature, and it is faster at higher final intracavity power [5, 8, 9, 14]. Here, we further investigate the temporal photo-birefringent response at 1542 nm with or without constant LED light in the visible and near infrared.

As the magnitude of the change depends on the step size, we normalize all the curves by the difference of initial $\Delta_{\text{biref}}(t_0)$ and final line splitting $\Delta_{\text{biref}}(t_{\text{final}})$

$$\delta_{\text{biref}}(t) = \frac{\Delta_{\text{biref}}(t) - \Delta_{\text{biref}}(t_{\text{final}})}{\Delta_{\text{biref}}(t_0) - \Delta_{\text{biref}}(t_{\text{final}})}, \quad (5)$$

resulting in a normalized response of birefringence from 1 to 0 that was found to be independent of the initial power level and the step size of the power [9].

1. Without additional LED illumination

The transient responses of δ_{biref} to step changes of intracavity power is investigated. The half time of the transient response decreases from 1.3 s to 0.3 s when the final power P_{trans} is increased from 10 μW to 49 μW . Different from the observed temporal behavior at 124 K [5], here the splitting is monotonically approaching its final value. We find that the transient behavior can be best described by a sum of an exponential term representing the initial relaxation and a stretched exponential term

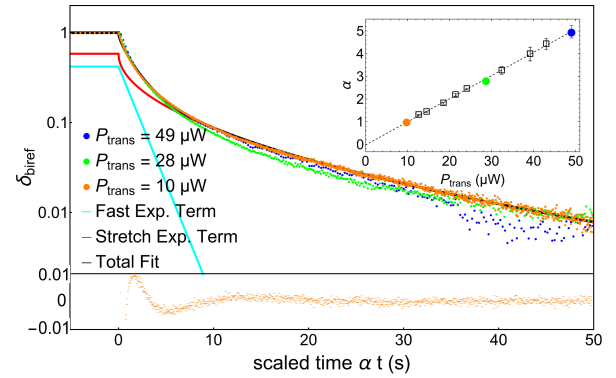


FIG. 4. Normalized transient response δ_{biref} to a step change of intracavity power without LED illumination. Responses of three final transmitted powers of 10 μW , 28 μW and 49 μW are shown. The time axes of the two curves at $P_{\text{trans}} = 28$ and 49 μW are scaled by $\alpha = 2.8$ and $\alpha = 5.0$ with respect to the slower curve at 10 μW (orange) ($\alpha = 1$). The response at 10 μW was fitted according to Eq. 6 with a sum of an exponential function (cyan) and a stretched exponential function (red) representing the slow part. The fit residuals are displayed in the lower panel. The inset displays the scaling factors α versus the final power P_{trans} for the curves in the main figure (circles) and at other power levels (open squares).

that describes the slow part of the curve Eq. 6:

$$\delta_{\text{biref}}(t) = A e^{-(\alpha t/\tau_1)^\beta} + (1 - A) e^{-\alpha t/\tau_2}. \quad (6)$$

First, a fit to the data at $P_{\text{trans}} = 10 \mu\text{W}$ ($\alpha = 1$) was performed, with weighting factor of $1/\delta_{\text{biref}}(t)$ to ensure a good fit across the whole decay. The fit gives a best exponent $\beta = 0.510(1)$ and relative amplitude $A = 0.579(4)$. The time constants of the stretched exponential and the normal exponential are $\tau_1 = 2.92(6)$ s and $\tau_2 = 1.65(1)$ s respectively. The stretched exponential behavior of δ_{biref} might be related to the observations of slow relaxation of photo carriers in persistent photo-conductivity of Al-GaAs, where the exponent β was found to be temperature dependent [22].

Next, only α in Eq. 6 was fit to the measurement at other P_{trans} with the other parameters fixed to the result of the initial fit. This corresponds to stretching the time axis by a factor of α to overlap all the curves (see Fig. 9 in the Supplementary Material). Fig. 4 shows two curves ($P_{\text{trans}} = 49 \mu\text{W}$ and 28 μW) with scaled time axis αt and the original curve at 10 μW that well overlap. The scaling factors α for a total of ten different P_{trans} with respect to the curve at final $P_{\text{trans}} = 10 \mu\text{W}$ is shown in the inset of Fig. 4. The uncertainties were obtained from fits with different weighting factors (see Supplementary Material). A linear fit to the scaling factor results in $\alpha = 0.102(1) \cdot P_{\text{trans}}/\mu\text{W} - 0.03(3)$.

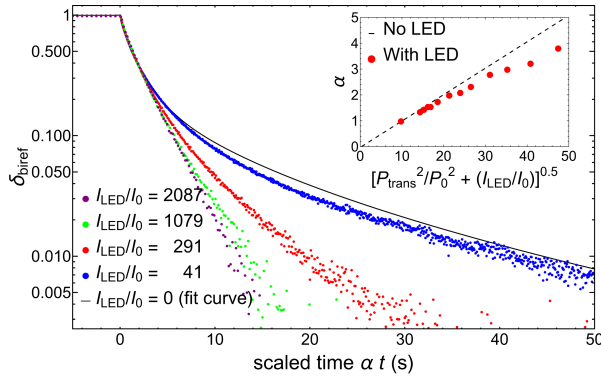


FIG. 5. Normalized transient response δ_{biref} to a step change of intracavity power (corresponding to $P_{\text{trans}} = 11.0 \mu\text{W}$ to $12.8 \mu\text{W}$) at different values of I_{LED} at 535 nm. The time axis is scaled by a factor α compared to the axis without LED illumination (see text). The same step change in intracavity power without LED is shown as reference (black). The inset displays α as a function of transmitted power P_{trans} and LED intensity I_{LED} at fixed $P_{\text{trans}} = 12.8 \mu\text{W}$ (red) and without LED, varying P_{trans} (black dashed as in the inset of Fig. 4).

2. With additional constant LED illumination

Next we investigate the temporal response to a change in intracavity power, when the mirrors are additionally illuminated by LED light at fixed intensities. The same 535 nm green LED is used as before. We measure the transient responses of the line splitting to a change of intracavity power, corresponding to $P_{\text{trans}} = 11.0 \mu\text{W}$ to $12.8 \mu\text{W}$. We try to overlap the normalized responses obtained at different LED intensities (see Fig. 10 in the Supplementary Material) by stretching the time axis. We observe that the curves cannot be overlapped: the long term behavior is very different. Nevertheless, we can overlap the curves at short times by stretching the time axis such that they agree at $\delta_{\text{biref}}(\alpha t) = 1/e$ (see Fig. 5), where $\alpha = 1$ refers to the same reference curve without LED as in Fig. 4.

This common reference allows us to compare the dependence of the scaling factors α on intracavity power and LED intensity (inset of Fig. 5). The factors are plotted versus the square root of quantity x (Eq. 1) that combines also the effects of intracavity power and the LED intensity in the steady state modification of the splitting. Both sets of α agree well at small values of \sqrt{x} . The deviation at high I_{LED} may be related to the different behavior of the two mirrors due to the different intracavity light and LED light intensities impinging on each.

V. TRANSIENT RESPONSE TO CHANGE OF LED INTENSITY

Finally, the temporal response of the photo-modified birefringence to a step of LED intensity at constant in-

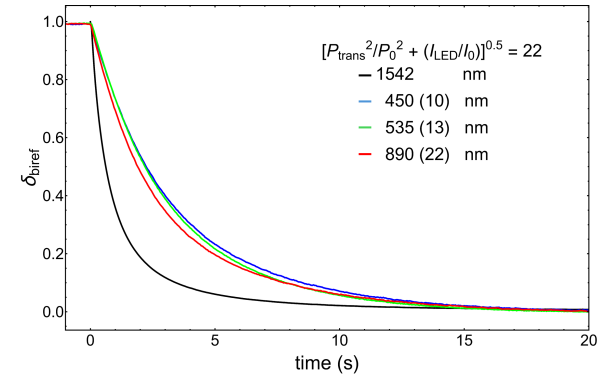


FIG. 6. Normalized transient response of δ_{biref} to switching on different LEDs at 450 nm (blue), 535 nm (green) and 890 nm (red). All measurements have the same intracavity power corresponding to $P_{\text{trans}} = 10.7 \mu\text{W}$ and the LED intensity was adjusted to lead to the same final splitting Δ_{biref} . For comparison the response to a step of intracavity power is shown by the black line. Here the power was stepped up from $P_{\text{trans}} = 10.7 \mu\text{W}$ to $22.0 \mu\text{W}$, leading to the same final splitting.

tracavity power was studied. Here also higher LED intensity results in a faster response (see Fig. 11 and 12 in Supplementary Material), similar to the behavior on intracavity power. We measure the responses of the normalized birefringent splitting to turning on LEDs (IR, green and blue) at constant intracavity power $P_{\text{trans}} = 10.7 \mu\text{W}$ and compare it to a step of intracavity power from $P_{\text{trans}} = 10.7 \mu\text{W}$ to $22.0 \mu\text{W}$ without LED (Fig. 6). The LED intensity was chosen to result in the same final splitting, independent of the wavelength. According to our model this corresponds to setting $\sqrt{x} = 22$ (Eq. 1).

The observed responses to LED light are much slower than the response to intracavity light (half time 0.7 s). This could be related to radial charge transport from the whole illuminated coating surfaces with radius of 3 mm to the area of the cavity mode at the mirrors with beam radii of 675 and 496 μm .

Only a small difference is observed between IR (half-time of 2.0 s) and blue/green light (halftime of 2.3 s), which could be due to the different charge transfer time when charges are created at different coating depths. The absorption coefficients of GaAs as function of wavelength [23] leads to predominant absorption of the blue and green LED light in the first few layers, whereas for the 890 nm LED light is absorbed throughout all coating layers (see Supplementary Table I).

VI. SUPPRESSION OF FREQUENCY NOISE INDUCED BY LASER POWER FLUCTUATIONS

Unavoidable absorption of the intracavity light leads to heating of mirror coatings and the mirror substrates underneath. Thus the thermal expansion of the coating and the substrate (thermo-elastic effect) and the temper-

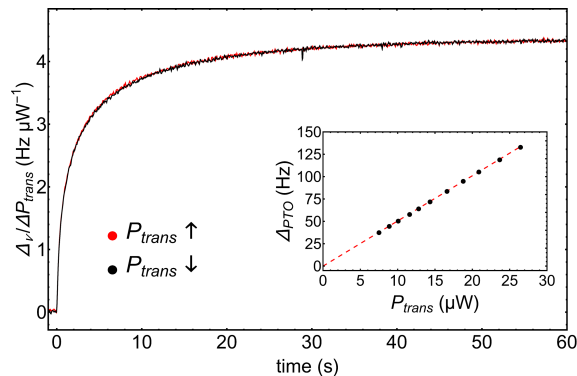


FIG. 7. Transient change of the average frequency of a fast and a slow cavity eigenmode Δ_{PTO} to a step of intracavity power from $P_{\text{trans}} = 9.2 \mu\text{W}$ up to $10.9 \mu\text{W}$ (red) and back down to $9.2 \mu\text{W}$ (black), normalized by the step size. The inset shows the steady-state frequency changes Δ_{PTO} as function of P_{trans} extrapolated to 0 with a linear fit shown in the dashed line.

ature dependent index of the coating material (thermo-refractive effect) will shift the resonance frequency of the cavity by Δ_{PTO} (subsumed as photo-thermo-optic (PTO) effect) [24]. To measure the PTO effect, we observe the average frequency change of the fast and the slow eigenmodes to a step in optical power (see Fig. 7). Because of the thermal expansion of the fused silica substrates, the cavity length shortens with increasing power. As expected from a pure thermal effect, the amplitude of the transient response from Δ_{PTO} is proportional to the step size of optical power (Fig. 7 inset) with slope $4.5 \text{ Hz}/\mu\text{W}$, equivalent to an optical length change of $5.6 \text{ fm}/\mu\text{W}$ of each mirror. In addition, the shape of the transient response, normalized to step size is independent of power, with 1.3 s halftime, similar to other cavities with AlGaAs coatings on fused silica substrates [8, 25].

Fluctuations of the intracavity power couple to cavity frequency ν via the PTO effect [26] and via the modification of the birefringence simultaneously. As the birefringence shows opposite signs on fast and slow axes, the corresponding frequency on the fast and slow axes at a certain power is given by

$$\nu_{\text{fast,slow}} = \nu_0 + \Delta_{\text{PTO}} \pm \Delta_{\text{biref}}/2, \quad (7)$$

where ν_0 is the unperturbed frequency. Thus, the overall effects of power induced frequency shifts partially cancel in one polarization mode [7, 8]. Good cancellation of frequency noise due to power fluctuations thus requires well matched temporal responses of PTO and birefringent effects.

Different from the PTO, the slope of the birefringent splitting versus intracavity power (Fig. 2) strongly depends on intracavity power. For example, at $P_{\text{trans}} = 52 \mu\text{W}$ the slope of half the birefringent splitting is similar to the slope of Δ_{PTO} with power.

Because the time constants of the two effects are generally different the compensation cannot be perfect and

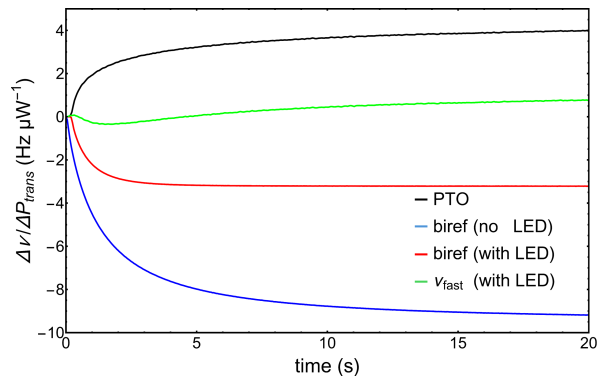


FIG. 8. Contributions to the resonance frequency changes upon a step in intracavity power from photo-thermo-optic effect (black) and from the photo birefringent effect without (blue) and with constant LED illumination at 535 nm (red). The total shift for the fast axis with LED illumination is shown in green.

some sensitivity to power fluctuations remains [7, 8]. In this case at $52 \mu\text{W}$, a residual power sensitivity around $0.5 \text{ Hz}/\mu\text{W}$ to a small step change in intracavity power remains. Thus, to further minimize the frequency noise it would be advantageous to operate at lower power where the absolute power fluctuations are smaller. However, according to our model, lowering the power increases the slope of the birefringent splitting above the constant slope of Δ_{PTO} , and the compensation degrades.

LED irradiation offers another degree of freedom to optimize the cancellation at a lower optical power. To demonstrate this method we choose here a low intracavity power of $P_{\text{trans}} = 11 \mu\text{W}$, where the sensitivity amounts to $4 \text{ Hz}/\mu\text{W}$ without LED light. The LED intensity was optimized that the photo-birefringent frequency change almost counteracts Δ_{PTO} after a step in laser power (Fig. 8). The residual sensitivity is below $0.5 \text{ Hz}/\mu\text{W}$ for up to 10 s after the power step, which is very similar to the case when a operating power level is chosen at $P_{\text{trans}} = 52 \mu\text{W}$. Assuming constant fractional power stability, reducing the laser power by a factor of 4.5 reduces the corresponding frequency noise by the same factor. Operating at lower power would even further reduce the noise.

VII. CONCLUSION AND OUTLOOK

From the investigations of the photo-birefringent effects of crystalline AlGaAs coatings at room temperature we have derived a model that is based on two processes. In the first process light creates charges by photoabsorption. The modification of birefringence is much stronger for LED light above the bandgap of GaAs and also shows different dependence on power compared to intracavity light below the bandgap of GaAs. This suggests an initial single photon absorption by GaAs for short wavelengths, in contrast to two photon absorption for long

wavelengths.

In the next process the charge carriers generated by photon absorption diffuse and modify the birefringence by electro-optic effect or by photo-plastic effect. The normalized transient response mostly depends on the final modification of the birefringence, with or without LED illumination. This suggests that the response is limited by the dynamics of the second process, like charge diffusion, while the first process happens much faster.

Crystalline coatings offer the possibility for next generation room temperature cavities aiming at 1×10^{-17} fractional frequency instability due to the low thermal noise floor. At this level, coupling of laser power noise to frequency noise is still a technical challenge. For example, in state of the art room temperature cavities with AlGaAs coatings, laser power noise contributes to the instability up to $3 - 4 \times 10^{-17}$ even with active power stabilization and choosing the polarization with the smaller sensitivity, where photo-thermo-optic effect and photo birefringent effect partially cancel [7, 27]. The better understanding of the light induced birefringence obtained in our investigations offers the possibility a similar cancellation at a much lower laser power level by adding LED illumination. As the fractional power stability typically remains the same, operating at lower power thus opens a pathway towards low thermal noise limited instability.

Extending our investigations of the photo-birefringent effects to other temperatures and with well controlled area of illumination would be useful. In addition, investigations on the inherent novel coating noise processes would be needed to understand the best performance of AlGaAs coatings at room temperature.

VIII. ACKNOWLEDGEMENTS

We acknowledge support by the Project 20FUN08 NEXTLASERS, which has received funding from the EMPIR programme cofinanced by the Participating States and from the European Union's Horizon 2020 Research and Innovation Programme, and by the Deutsche Forschungsgemeinschaft (DFG, German Research Foundation) under Germany's Excellence Strategy—EX-2123 QuantumFrontiers (Project No. 390837967), SFB 1227 DQ-mat (Project No. 274200144). This work is partially supported by the Max Planck-RIKEN-PTB Center for Time, Constants and Fundamental Symmetries. We thank Jun Ye and Dhruv Kedar for the insightful discussions.

IX. SUPPLEMENTARY MATERIAL

The following provides additional information on the wavelength dependent absorption of the crystalline coatings and transient frequency changes due to step changes in intracavity light at 1542 nm and to step changes of diffuse LED light ranging from 450 nm to 890 nm.

A. Wavelength-dependent coating absorption

We calculate the wavelength and spatially-dependent absorption in an $\text{Al}_{0.92}\text{Ga}_{0.08}\text{As}/\text{GaAs}$ coating from absorption coefficients of GaAs and $\text{Al}_{0.8}\text{Ga}_{0.2}\text{As}$ [23]. In the wavelength range of interest, the absorption of $\text{Al}_{0.92}\text{Ga}_{0.08}\text{As}$ can be neglected compared to the one of GaAs. We first calculate the absorption depth of GaAs (Table. I). The coatings consist of alternating GaAs (115.6 nm) and AlGaAs layers (133.2 nm), starting with GaAs. The blue and green light is absorbed mainly in the first two GaAs layers. For the IR light the absorption depth is larger than the coating thickness and light is absorbed throughout the whole coating (consisting of 38.5 pairs). 74% of the light is transmitted by the coating.

TABLE I. Wavelength-dependent absorption in the $\text{Al}_{0.92}\text{Ga}_{0.08}\text{As}/\text{GaAs}$ coating. The $1/e$ absorption depth of GaAs is shown in the second column [23] and the corresponding thickness in terms of layer pairs is estimated.

Wavelength	Absorption depth	Coating layers
459 nm	0.04 μm	1 pair
539 nm	0.13 μm	2 pairs
885 nm	15.38 μm	62 pairs

B. Transient response to intracavity power without additional LED illumination

We use Eq. 6 to fit the stretching factor α to the normalized transient line splitting due to a step change in intracavity power. Especially for the faster responses at higher power we observe that we cannot equally well fit the response at short and long time. By using a constant weight or a weight of $1/\delta_{\text{biref}}(t)$ in the fit we can achieve better agreement at short or longer times respectively. In the second case the maximum weight is limited to 100 to not give too much weight to noise. Fig. 9 displays the original $\delta_{\text{biref}}(t)$ data and the fitted curves for the two cases.

The inset in Fig. 4 displays the average value for the fitted alpha in the two cases and the error bars show the deviation between the two.

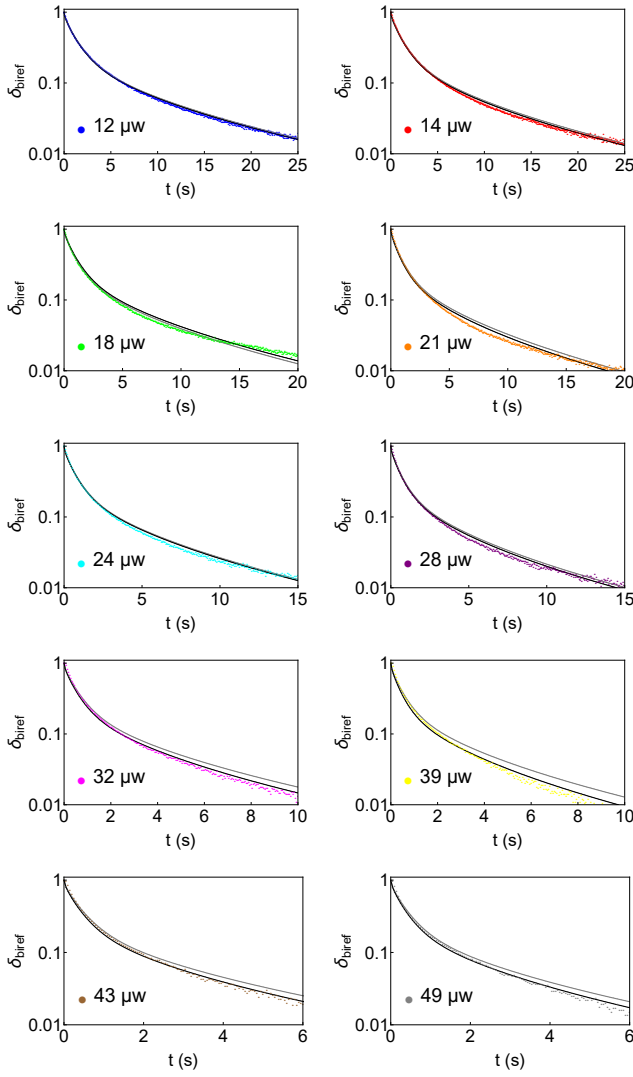


FIG. 9. Measured normalized transient behavior of line splitting $\delta_{\text{biref}}(t)$ at 10 different final transmission power. The lines display the fitting results with varying (black) and constant (gray) weighting factors.

C. Transient response to intracavity power with additional LED illumination

Fig. 10 shows the normalized transient response of a step change in cavity power ($P_{\text{trans}} = 11.0 \mu\text{W}$ to $12.8 \mu\text{W}$) at different LED intensities. At a higher constant LED intensity the response is faster, similar to the case of varying intracavity power. At very small LED intensity the transient behavior is similar to the response without LED.

D. Transient response to change of LED intensity

We also investigate the transient response to switching on a green LED for different final intensities. The nor-

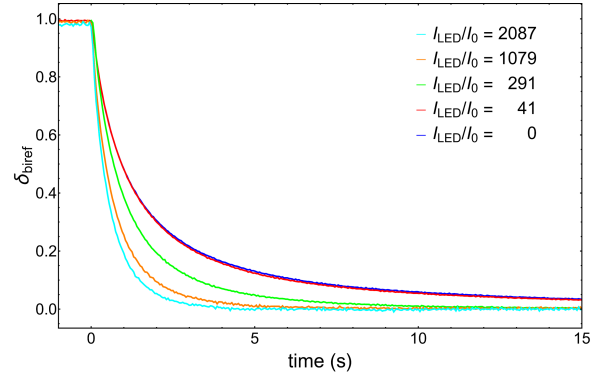


FIG. 10. Normalized transient response δ_{biref} to the same step of intracavity power from at $11.0 \mu\text{W}$ to $12.8 \mu\text{W}$ at four intensities I_{LED} of the green LED. At higher intensity, the transient response is faster. The transient response without LED light (blue) is shown for comparison.

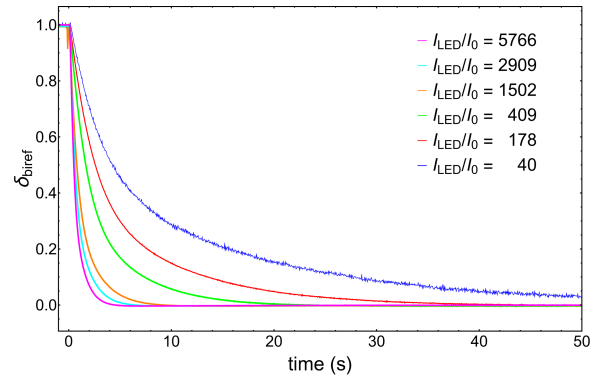


FIG. 11. Normalized transient responses of δ_{biref} to switching on a 535 nm LED to different final intensities I_{LED} with $I_0 = 3.4 \mu\text{W}/\text{m}^2$. The intracavity power was fixed to $P_{\text{trans}} = 12.5 \mu\text{W}$.

malized transient responses are shown in Fig. 11. Similar to the dynamic response to intracavity power, increasing the final LED intensity also accelerates the response.

We overlap the curves at short times by stretching the time axis such that they agree at $\delta_{\text{biref}}(\alpha t) = 1/e$, where $\alpha = 1$ refers to $(I_{\text{LED}}/I_0)^{0.5} = 10$. By scaling the time axis, as shown in Fig. 12, the initial decay of the curves can be overlapped. The scaling factors α are approximately proportional to the square root of (I_{LED}/I_0) as shown in the inset. At longer times a second exponential decay is visible. The time constant of the second exponential term decreases even faster with increasing LED intensity than the initial $1/e$ time constant.

REFERENCES

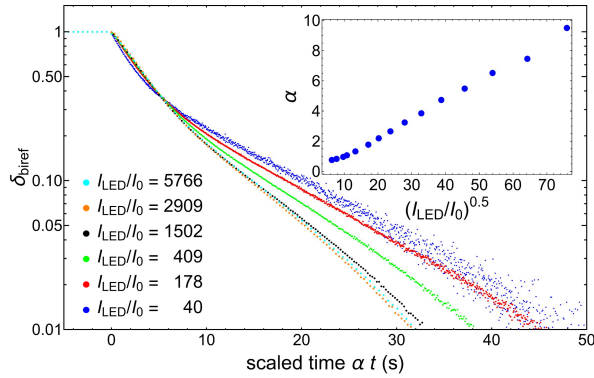


FIG. 12. Normalized transient response of δ_{biref} to switching on a 535 nm LED to different final intensities I_{LED} with $I_0 = 3.4 \mu\text{W}/\text{m}^2$. The intracavity power was fixed to $P_{\text{trans}} = 12.5 \mu\text{W}$. The time axis is scaled by a factor α compared to the curve with $(I_{\text{LED}}/I_0)^{0.5} = 10$ to match the initial part of the response for the different intensities. The inset shows the scaling factor α as a function of $(I_{\text{LED}}/I_0)^{0.5}$.

[1] A. D. Ludlow, M. M. Boyd, J. Ye, E. Peik, and P. O. Schmidt, Optical atomic clocks, *Rev. Mod. Phys.* **87**, 637 (2015).

[2] G. M. Harry, H. Armandula, E. Black, D. R. M. Crooks, G. Cagnoli, J. Hough, P. Murray, S. Reid, S. Rowan, P. Sneddon, M. M. Fejer, R. Route, and S. D. Penn, Thermal noise from optical coatings in gravitational wave detectors, *Appl. Opt.* **45**, 1569 (2006).

[3] M. Granata, A. Amato, G. Cagnoli, M. Coulon, J. Degallaix, D. Forest, L. Mereni, C. Michel, L. Pinard, B. Sassolas, and J. Teillon, Progress in the measurement and reduction of thermal noise in optical coatings for gravitational-wave detectors, *Appl. Opt.* **59**, A229 (2020).

[4] G. D. Cole, W. Zhang, B. J. Bjork, D. Follman, P. Heu, C. Deutsch, L. Sonderhouse, J. Robinson, C. Franz, A. Alexandrovski, M. Notcutt, O. H. Heckl, J. Ye, and M. Aspelmeyer, High-performance near- and mid-infrared crystalline coatings, *Optica* **3**, 647 (2016).

[5] J. Yu, S. Häfner, T. Legero, S. Herbers, D. Nicolodi, C. Y. Ma, F. Riehle, U. Sterr, D. Kedar, J. M. Robinson, E. Oelker, and J. Ye, Excess noise and photoinduced effects in highly reflective crystalline mirror coatings, *Phys. Rev. X* **13**, 041002 (2023).

[6] D. Kedar, J. Yu, E. Oelker, A. Staron, W. R. Milner, J. M. Robinson, T. Legero, F. Riehle, U. Sterr, and J. Ye, Frequency stability of cryogenic silicon cavities with semiconductor crystalline coatings, *Optica* **10**, 464 (2023).

[7] B. Kraus, S. Herbers, C. Nauk, U. Sterr, C. Lisdat, and P. O. Schmidt, Ultra-stable transportable ultraviolet clock laser using cancellation between photo-thermal and photo-birefringence noise, *Opt. Lett.* **50**, 658 (2025).

[8] X.-Q. Zhu, X.-Y. Cui, D.-Q. Kong, H.-W. Yu, X. Jiang, P. Xu, H.-N. Dai, Y.-A. Chen, and J.-W. Pan, Photo-birefringent effects of crystalline coatings in ultra-stable cavities, in *Fourteenth International Conference on Information Optics and Photonics (CIOP 2023)*, Vol. 12935, edited by Y. Yang, International Society for Optics and Photonics (SPIE, 2023) p. 1293541.

[9] C. Y. Ma, J. Yu, T. Legero, S. Herbers, D. Nicolodi, M. Kempkes, F. Riehle, D. Kedar, J. M. Robinson, J. Ye, and U. Sterr, Ultrastable lasers: investigations of crystalline mirrors and closed cycle cooling at 124 K, *J. Phys.: Conf. Ser.* **2889**, 012055 (2024).

[10] B. Wu, S. Goswami, S. Tanioka, and S. Ballmer, Birefringence of AlGaAs/GaAs coatings under above-band-gap illumination, GR noise and photo-optic transfer function, arXiv:2512.00594 [physics.ins-det] (2025), IIGO Document P2500676-v2.

[11] S. Häfner, S. Falke, C. Grebing, S. Vogt, T. Legero, M. Merimaa, C. Lisdat, and U. Sterr, 8×10^{-17} fractional laser frequency instability with a long room-temperature cavity, *Opt. Lett.* **40**, 2112 (2015).

[12] G. D. Cole, S. Ballmer, G. Billingsley, S. B. Cataño Lopez, M. Fejer, P. Fritschel, A. M. Gretarsson, G. M. Harry, D. Kedar, T. Legero, C. Makarem, S. D. Penn, D. Reitze, J. Steinlechner, U. Sterr, S. Tanioka, G. W. Truong, J. Ye, and J. Yu, Substrate-transferred GaAs/AlGaAs crystalline coatings for gravitational-wave detectors, *Appl. Phys. Lett.* **122**, 110502 (2023).

[13] T. Legero, T. Kessler, and U. Sterr, Tuning the thermal expansion properties of optical reference cavities with fused silica mirrors, *J. Opt. Soc. Am. B* **27**, 914 (2010).

[14] B. Kraus, *A highly stable UV clock laser*, Ph.D. thesis, QUEST-Leibniz-Forschungsschule der Gottfried Wilhelm Leibniz Universität Hannover (2023).

[15] J. Yu, *Cryogenic silicon Fabry-Perot resonator with Al_{0.92}Ga_{0.08}As/GaAs mirror coatings*, Ph.D. thesis, QUEST-Leibniz-Forschungsschule der Gottfried Wilhelm Leibniz Universität Hannover (2023).

[16] D. G. Matei, T. Legero, S. Häfner, C. Grebing, R. Weyrich, W. Zhang, L. Sonderhouse, J. M. Robinson, J. Ye, F. Riehle, and U. Sterr, 1.5 μm lasers with sub-10

mHz linewidth, Phys. Rev. Lett. **118**, 263202 (2017).

[17] S. Adachi, Elastooptic and electrooptic effect, in *Physical Properties of III-V Semiconductor Compounds* (John Wiley & Sons, Ltd, 1992) Chap. 9, pp. 193–222.

[18] S. Koubaiti, J. Couderc, C. Levade, and G. Vanderschaeve, Photoplastic effect and Vickers microhardness in III-V and II-VI semiconductor compounds, Mater. Sci. Eng. A **234-236**, 865 (1997).

[19] B. E. Mdivanyan and M. S. Shikhsaidov, Photostimulated enhancement of dislocation glide in gallium arsenide crystals, physica status solidi (a) **107**, 131 (1988).

[20] G. Winkler, L. W. Perner, G.-W. Truong, G. Zhao, D. Bachmann, A. S. Mayer, J. Fellinger, D. Föllman, P. Heu, C. Deutsch, D. M. Bailey, H. Peelaers, S. Puchegger, A. J. Fleisher, G. D. Cole, and O. H. Heckl, Mid-infrared interference coatings with excess optical loss below 10 ppm, Optica **8**, 686 (2021), see erratum: <https://doi.org/10.1364/OPTICA.520398> [28].

[21] W. Shockley, The theory of p-n junctions in semiconductors and p-n junction transistors, Bell Sys. Tech. J. **28**, 435 (1949).

[22] S. Ghosh, Slow relaxation of nonequilibrated photo-carriers in semiconductors, Phase Transitions **77**, 791 (2004).

[23] D. E. Aspnes, S. M. Kelso, R. A. Logan, and R. Bhat, Optical properties of $\text{Al}_x\text{Ga}_{1-x}\text{As}$, J. Appl. Phys. **60**, 754 (1986).

[24] A. Farsi, M. Siciliani de Cumis, F. Marino, and F. Marin, Photothermal and thermo-refractive effects in high reflectivity mirrors at room and cryogenic temperature, J. Appl. Phys. **111**, 043101 (2012).

[25] S. Herbers, *Transportable ultra-stable laser system with an instability down to 10^{-16}* , Ph.D. thesis, QUEST-Leibniz-Forschungsschule der Gottfried Wilhelm Leibniz Universität Hannover (2021).

[26] M. De Rosa, L. Conti, M. Cerdonio, M. Pinard, and F. Marin, Experimental measurement of the dynamic photothermal effect in Fabry-Perot cavities for gravitational wave detectors, Phys. Rev. Lett. **89**, 237402 (2002).

[27] X.-Q. Zhu, X.-Y. Cui, D.-Q. Kong, H.-W. Yu, X.-M. Zhai, M.-Y. Zheng, X.-P. Xie, Q. Zhang, X. Jiang, X.-B. Zhang, P. Xu, H.-N. Dai, Y.-A. Chen, and J.-W. Pan, An ultrastable 1397-nm laser stabilized by a crystalline-coated room-temperature cavity, Rev. Sci. Instrum. **95**, 083002 (2024).

[28] L. W. Perner, G. Winkler, G.-W. Truong, G. Zhao, D. Bachmann, A. S. Mayer, J. Fellinger, D. Föllman, P. Heu, C. Deutsch, D. M. Bailey, H. Peelaers, S. Puchegger, A. J. Fleisher, G. D. Cole, and O. H. Heckl, Mid-infrared interference coatings with excess optical loss below 10 ppm: erratum, Optica **11**, 619 (2024).